Article

Correlating Mechanical Sensitivity with Spin Transition in the Explosive Spin Crossover Complex [Fe(Htrz)][ClO]

Thuy-Ai D. Nguyen, Jacqueline M. Veauthier, Gary F Angles-Tamayo, David E Chavez, Ekaterina Lapsheva, Thomas W. Myers, Tammie R. Nelson, and Eric J. Schelter

J. Am. Chem. Soc., **Just Accepted Manuscript** • DOI: 10.1021/jacs.9b13835 • Publication Date (Web): 13 Feb 2020

Correlating Mechanical Sensitivity with Spin Transition in the Explosive Spin Crossover Complex $[Fe(Htrz)_3]_n[ClO_4]_{2n}$

Thuy-Ai D. Nguyen,*,† Jacqueline M. Veauthier,*,† Gary F. Angles-Tamayo,† David E. Chavez,† Ekaterina Lapsheva,‡ Thomas W. Myers,†,§ Tammie R. Nelson,† Eric J. Schelter ‡

†Explosive Science and Shock Physics, Chemistry, and Theoretical Divisions, Los Alamos National Laboratory

‡Department of Chemistry, University of Pennsylvania

ABSTRACT: Spin crossover complexes are known to undergo bond length, volume and enthalpy changes during spin transition. In an explosive spin crossover complex, these changes could affect the mechanical and initiation sensitivity of the explosive and lead to the development of a new class of sensitivity switchable materials. To explore this relationship, the well-known spin crossover compound $[Fe(Htrz)_3]_n[ClO_4]_{2n}$ (**1**) was re-evaluated for its explosive properties and its mechanical impact sensitivity was correlated to spin transition. A variable temperature impact test was developed and used to evaluate the impact sensitivity of **1** in the low spin (LS, S=0), and thermally accessed high spin (HS, S=2) and mixed LS and HS states. For comparison, the structurally similar Ni compound, $[Ni(Htrz)_3]_n[ClO_4]_{2n}$ (**2**), that does not undergo a spin transition at accessible temperatures, was synthesized and characterized and its explosive properties and variable temperature impact sensitivity measured. These results reveal a correlation between impact sensitivity and spin transition, where **1** exhibits lower impact sensitivity in the LS state and increases in sensitivity upon transition to the HS state. Density functional theory was used to predict structural changes that occur upon spin transition that correlate to the change in sensitivity. This demonstrates, for the first time, an explosive spin crossover compound (ExSCO) that exhibits switchable impact sensitivity with a fully reversible internal switching mechanism.

Introduction

Spin crossover (SCO) is a phenomenon in transition metal complexes that has garnered interest for use in switching devices, sensors and displays.[1-3] These SCO compounds exhibit bistability at a molecular level where the metal center undergoes a spin transition, most commonly from a low spin (LS) to a high spin (HS) electronic configuration at a critical temperature, resulting in a change in the magnetic, structural and optical properties of the material.[1, 2, 4] A spin transition can occur in response to both thermal and non-thermal stimuli, including magnetic fields, pressures, and irradiation with light, which all alter the critical temperature of the spin state transition.[2, 5-10] The most viable potential applications for SCO materials in electronic devices require that the spin transition occurs with a wide hysteresis loop and at a critical temperature close to room temperature.[1, 2, 4, 11] The coordination polymers $[Fe(Htrz)_{3-n}(trz)_n]X_{2-n}$ (trz = 1,2,4-triazolate or a 4-substituted derivative, X^- is a mono-anion, and $0 \leq n \leq 1$) are amongst the most widely studied and promising of the SCO compounds with this combination of properties.[1-4, 11-13] Notably, $[Fe(Htrz)_{3-n}(trz)_n]X_{2-n}$ systems have nitrogen-rich ligands and often contain perchlorate counterions resulting in energy dense and potentially explosive materials.[3, 14-20] While the explosive properties of these compounds have not been studied, we contend there is potential for significant application for explosive spin crossover (ExSCO) complexes as switchable explosives.

Switchable explosives with on-demand mechanical sensitivity are highly desirable for their potential to revolutionize explosives safety. The ideal system being one that can reliably undergo a reversible phase change between a safe phase that is insensitive (or has low sensitivity) and an active phase that is sensitive towards destructive stimuli and will detonate reliably. Spin transitions in SCO compounds typically result in volume (2-5%) and enthalpy (6-15 kJ/mol) changes.[1-3] Certain conventional explosives are known to exhibit phase transitions that are accompanied by similar volume and enthalpy changes as well as changes in mechanical sensitivity. For example, the conventional explosive, HMX, has a phase change between 158-190°C as it switches from β-HMX (chair conformation) to δ-HMX (boat conformation).[21, 22] Relative to the β-HMX phase, the δ-HMX phase has a 6% lower density, an enthalpy of formation that is +8.9 kJ/mol, and, most importantly is more sensitive towards destructive stimuli.[21, 22] While this phase change results in a sensitivity switch, it is not reversible and the high temperatures required to achieve this transition make HMX untenable as a switchable explosive.[21, 22] In contrast, there are SCO materials that have reversible solid-state phase transitions at accessible temperatures and pressures.[2, 23, 24] These spin transitions result in volume expansion (2-5%) and enthalpy changes (6-15 kJ/mol) comparable to those observed in the β-HMX to δ-HMX phase transition that results in a sensitivity change.[1, 2, 21, 22] Thus, carefully designed ExSCO materials should also exhibit

sensitivity changes when transitioned between spin states. We now report the explosive properties of the previously prepared SCO complex $[Fe(Htrz)_3]_n[ClO_4]_{2n}$ (**1**) and the new complex $[Ni(Htrz)_3]_n[ClO_4]_{2n}$ (**2**). Compound **1** has been shown to have reversible spin crossover.[14] We independently measured the magnetism of **1** and **2** and correlate the variable temperature impact sensitivity of **1** to spin crossover. We used density functional theory (DFT) to understand how the structural and energy changes that occur upon spin transition correlate to changes in sensitivity.

Results and Discussion

Synthesis. The SCO compound, $[Fe(Htrz)_3]_n[ClO_4]_{2n}$ (**1**), was synthesized according to a literature procedure (Scheme 1) such that three equiv. of 1,2,4-triazole (Htrz) in MeOH was added to a solution of iron (II) perchlorate hydrate in the presence of a small amount of ascorbic acid to minimize oxidation of Fe (II).[14] After stirring for 30 min, the solvent was removed under reduced pressure while heating in a 60 °C water bath and **1** was isolated in 98% yield as a purple powder. Notably, the complete removal of solvent by evaporation is important. Although it is not noted in the literature procedure, we found that material isolated by filtration, after concentration of the reaction solution, resulted in a purple powder that was lighter in color than **1** and did not exhibit a color change to off-white after heating to 90 °C.

Scheme 1. Synthesis of $[Fe(Htrz)_3]_n[ClO_4]_{2n}$ (1).

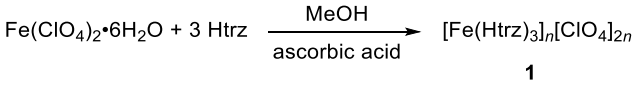

As a control, the previously unknown $[Ni(Htrz)_3]_n[ClO_4]_{2n}$ (**2**) was synthesized under similar conditions to that of **1**. Complex **2** is expected to be isostructural to **1** but, as a d^8 octahedral complex, it cannot undergo spin crossover. Three equiv. of Htrz in MeOH were added to a solution of nickel(II) perchlorate hydrate. No ascorbic acid was used due to the high stability of Ni(II) under these conditions. Upon addition of ligand, the green solution of the nickel salt immediately turned blue. After stirring for 30 min, the solvent was removed under reduced pressure while heating in a 60 °C water bath and **2** was isolated in 96% yield as a purple powder. Syntheses of both **1** and **2** were performed under dilute conditions to prevent precipitation of solid material before the reaction is complete. Compounds **1** and **2** isolated in this manner were found to be insoluble in a variety of solvents including MeOH, H_2O, acetone, alcohols, acetonitrile, nitromethane, dimethylformamide, dimethylsulfoxide, and dichloromethane. This insolubility is consistent with **1** and **2** forming polymeric structures (Figure 1). In addition, the blue color of the reaction and resultant purple powder supports the proposed octahedral geometry of the Ni center. There is a strong correlation between color and structure in most Ni(II) complexes, where Ni(II) octahedral complexes are typically blue, green, or violet, and Ni(II) square planar complexes are primarily yellow, orange or red.[25]

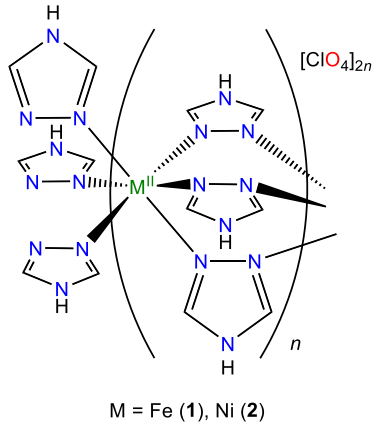

Figure 1. Diagram showing proposed connectivity in complexes $[Fe(Htrz)_3]_n[ClO_4]_{2n}$ (**1**) and $[Ni(Htrz)_3]_n[ClO_4]_{2n}$ (**2**).

Infrared Spectroscopy. Due to the insolubility of **1** and **2**, attempts to grow X-ray quality crystals were not successful and solution NMR was not obtained. Thus, we used infrared (IR) spectroscopy to establish structural similarities between **1** and **2** and to distinguish between the possible bonding modes and geometries in the 1,2-4-triazole (Htrz)/triazolate (trz) ligand. We also prepared $[Fe(Htrz)_2(trz)]_n[BF_4]_{2n}$ (**3**) according to a literature procedure[26] and measured its IR spectra for comparison to **1** and **2** because **3** has been structurally characterized as having both Htrz and trz ligands,[27] while **1** and **2** should only have Htrz ligands. Haasnoot and coworkers have made detailed IR spectra assignments for 1,2,4-triazole/triazolate and subsequent transition metal complexes with the goal of identifying predictive structural features.[28, 29] By using symmetry elements of known structures and the corresponding IR spectra, they determined that the absence or strongly reduced intensity of one of the two ring torsion vibration absorptions (τ1 and τ2) between 600 and 700 cm^{-1} indicates the Htrz and trz ligands have C_{2v} symmetry. Haasnoot *et al.* found that for free Htrz, τ1 and τ2 absorb at 682 and 649 cm^{-1}, repectively.[28] They also report only one strong absorption in the 600-700 cm^{-1} region for measured metal complexes having three Htrz ligands per metal (and no trz) and a single absorption near 680 cm^{-1} for μ_2-*N*1,*N*2-trz which also has C_{2v} symmetry.

Our IR spectra of complexes **1** and **2** each have only one feature assignable to a ring torsion vibration, at 626 cm^{-1} (Table 1, Figure 2). This establishes that both **1** and **2** have three bridging HTrz ligands per metal center with C_{2v} symmetry and no trz ligands. De Waal *et al.* previously reported the room temperature IR spectrum of compound **1** and the absorption at 630 cm^{-1} compares well with our data and is assigned to a ring torsion vibration, as well as to an overlapping ClO_4^- vibration.[30]

Table 1. Selected infrared spectra assignments for Htrz, Trz and complexes 1–3.

	τ1 (cm^{-1})	τ2 (cm^{-1})
HTrz (1,2,4-triazole)	682 (s)	649 (s)
Trz (1,2,4-triazolate)[28]	680 (s)	absent

$[Fe(Htrz)_3]_n[ClO_4]_{2n}$ (**1**)	absent	626 (s)
$[Fe(Htrz)_2(trz)]_n[BF_4]_{2n}$ (**3**)	633 (m)	680 (m)
$[Ni(Htrz)_3]_n[ClO_4]_{2n}$ (**2**)	absent	626 (s)

τ = ring torsion vibration.

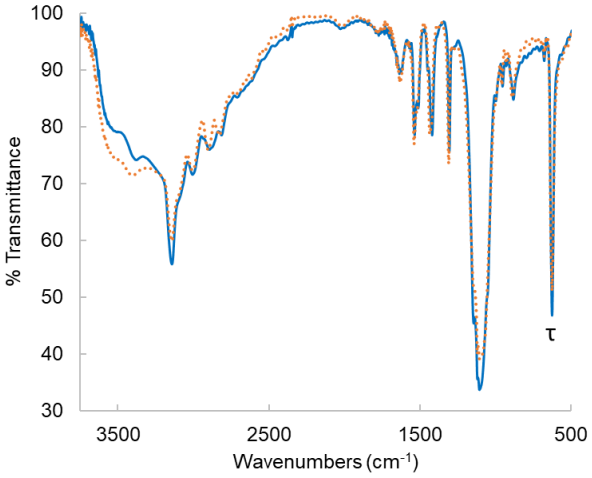

Figure 2. IR spectra of $[Fe(Htrz)_3]_n[ClO_4]_{2n}$ (**1**, solid blue line) and $[Ni(Htrz)_3]_n[ClO_4]_{2n}$ (**2**, dotted orange line). The absorption assigned to a ring torsion vibration is denoted as τ.

In summary, the IR spectra of **1** and **2** contain the same features and overlay almost perfectly, which is strong evidence that the two compounds are isostructural. Finally, the simplified spectrum of **1** and **2** as compared to both free Htrz and **3** is consistent with the symmetric polymeric structure proposed for **1** and **2** containing only one ligand environment (*viz.* bridging Htrz).

Magnetism. Magnetic susceptibility measurements of $[Fe(Htrz)_3]_n[ClO_4]_{2n}$ (**1**) were performed on powdered samples, diluted with KBr, in a 1 T applied field to detect the spin crossover behavior (Figure 3). Upon warming the sample from 250 K to 350 K, we observed a sharp increase of the χT product from 0.8 to 3.1 emu K mol^{-1}, consistent with a transition from the low spin state $^1A_{1g}$ to the high spin state $^5T_{2g}$. The $T_{1/2}\uparrow$ (warming) was 320 K. The χT value gradually increased before reaching a plateau with a value of 3.5 emu K mol^{-1}. Upon cooling the sample from 355 K to 250 K, the sharp decrease of the χT value signified the onset of spin crossover. The $T_{1/2}\downarrow$ (cooling) was 288 K. The observed spin crossover behavior is similar to the phenomena previously reported for other iron spin crossover compounds and iron-containing heterometallic phases.[1, 2, 31]

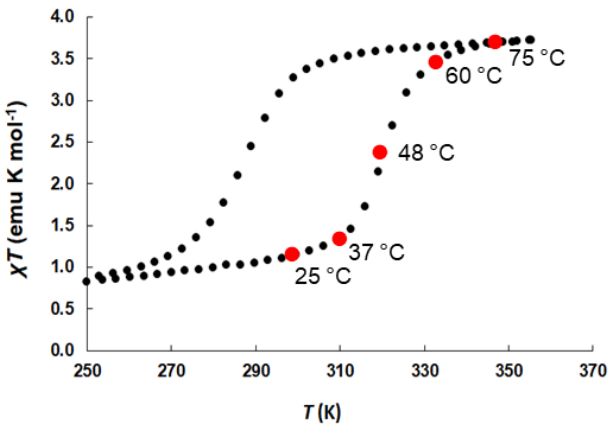

Figure 3. Temperature dependence of the χT product of $[Fe(Htrz)_3]_n[ClO_4]_{2n}$ (**1**) from 250 to 355 K interval in 1 T field. Red dots are associated to the corresponding temperature in °C.

As in the case of **1**, magnetic susceptibility measurements were performed on powdered samples of $[Ni(Htrz)_3]_n[ClO_4]_{2n}$ (**2**) diluted in a KBr matrix. In contrast to **1**, no spin crossover behavior was detected for **2**, as expected for the d^8 electronic configuration of the metal ion in an octahedral ligand field (Figure S5). The χT value of 1.1 is close to the spin-only value of 1, consistent with the presence of two unpaired electrons.

Thermal Stability and Room Temperature Mechanical Sensitivity. The thermal stabilities of **1** and **2** were evaluated through differential scanning calorimetry (DSC, Figures S6-7, and Table 2). Complex **1** has a broad decomposition exotherm with an onset at 198 °C, and three peaks at 225, 250 and 300 °C (Figure S6). The last peak at 300 °C being the most intense. Complex **2** is significantly more thermally stable than **1**. The DSC of **2** has a broad decomposition exotherm with an onset at 337 °C and peaks at 409 and 436 °C, but is still releasing heat and is not fully decomposed at the maximum DSC temperature of 450 °C.

Because water content is known to affect temperature dependent magnetic behavior and mechanical impact sensitivity measurements, we carefully monitored the amount of H_2O present per monomer unit for both **1** and **2** prior to all experiments where H_2O may have an effect (i.e., EA analysis and sensitivity testing).

Oxygen balance and explosive sensitivity data for **1** and **2** are listed in Table 2. Complex **2** has a slightly better oxygen balance (i.e., that is the degree to which an explosive can be oxidized) than **1** but both complexes are not as well balanced in oxygen when compared to the standard explosive, PETN (pentaerythritol tetranitrate).[32] At ambient temperatures, for impact and friction, **1** and **2** have similar sensitivities but are less sensitive (safer) than PETN. For spark (electrostatic discharge, ESD), complex **1** is more sensitive than **2** but similar in sensitivity to PETN.

Table 2. Decomposition temperatures, oxygen balance, and mechanical sensitivities of 1 and 2 compared to PETN.

	1·1.03H_2O	**2**·1.26H_2O	PETN

T_{dec} (°C)[a]	198	337	168
T_p (°C)[b]	225, 250, 300	409, 436	207
Ω_{CO_2} (%)[c]	—34.6	—32.7	—10.1
Ω_{CO} (%)[d]	—13.9	—12.0	15.2
Impact (J)[e]	7.86 ± 1.32	8.75 ± 1.2	2.99 ± 0.27
ESD (J)[f]	0.0625	0.125	0.0625
Friction (N)[g]	327.4 ± 41.8	333.2 ± 28.3	63.1 ± 10.8

[a]T_{dec} = onset temperature of decomposition from DSC. [b]T_p = peak(s) exotherm(s) from DSC. [c]Ω_{CO_2} = oxygen balance to CO_2 (a value of zero indicates perfectly balanced). [d]Ω_{CO} = oxygen balance to CO. [e]Impact sensitivity in joules. [f]Electrostatic discharge/static sensitivity. [g]Friction sensitivity.

Variable Temperature Impact Sensitivity at LS and HS States. The variable temperature (VT) impact sensitivities of **1** and **2** were measured to determine if the SCO behavior of **1** correlates to mechanical sensitivity. The LS to HS switch can be thermally accessed and has been shown to occur with reversible lengthening of the metal to ligand bonds. This weakening of the Fe-N bonds is expected to result in a lower initiation threshold for **1** in the HS state, as compared to the LS state.

To facilitate VT impact studies, we designed a VT collar for the anvil of our drop weight impact apparatus (Figure 4). The collar was machined from aluminum with an inlet and outlet (for attachment to a heater-chiller recirculating bath) and fitted with Viton O-rings. Grit paper was not used for our VT tests due to poor heat transfer through the grit from the anvil to the powder samples. Impact test temperatures of 25, 37, 48, 60, and 75 °C were chosen using the magnetic susceptibility data (*vide supra*) so that **1** was in the LS state at 25 and 37 °C, in a mixed LS/HS state at approximately the $T_{1/2}\uparrow$ temperature of 48 °C ($T_{1/2}\uparrow$ = 47 °C), almost fully in the HS state at 60 °C, and in the HS state at 75 °C. The switch to the HS state on the anvil was confirmed by a color change from purple to white (Figure 4a–b).

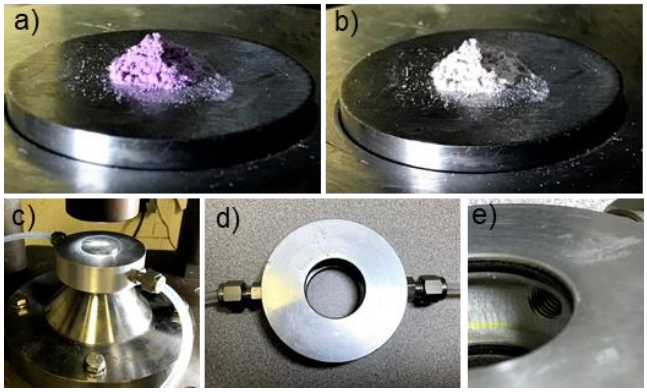

Figure 4. Images of 40 mg of $[Fe(Htrz)_3]_n[ClO_4]_{2n}$ (**1**) on the anvil of the LANL Type 12b Drop Weight Impact Machine with VT collar. a) 25 °C, showing **1** in the purple LS state b) 75 °C, showing **1** in the white HS state c) VT collar attached to anvil and recirculating bath d) VT collar exterior e) VT collar interior showing inlet/outlet and top/bottom O-rings.

Acoustic detection using two microphones (Bruel & Kjaer 4136) and two sound level meter (Bruel & Kjaer 2231) assemblies, set to capture max impulse RMS (root-mean-square) pressure levels, were employed for each drop. A go /no-go determination threshold of 105 dB was used to determine reaction or no reaction for each drop. These data were used to calculate the 50% drop height (H_{50}), the drop height at which, statistically, there is a reaction 50% of the time. The H_{50} was then converted to the corresponding impact sensitivity in joules, which is the energy at impact of the 2.5 kg drop weight.[33] The results are shown in Figure 5 and Table 3. At 25 and 37 °C, the impact sensitivity of **1** and **2** are indistinguishable within error. There is a drop in sensitivity going from 37 to 48 °C of 8.21 ± 0.78 J to 4.36 ± 2.47 J. 48 °C is the $T_{1/2}\uparrow$ where **1** is rapidly switching from LS to HS and is in a mixed spin state. Notably, the large sigma value of 2.47 J corresponds to the large range of 8 cm (drop heights: 22 – 30 cm) where there were both goes and no goes for the same drop height (range is 3 – 5 cm in impact data collected at other temperatures for **1**). This can be rationalized by the compound being close to the $T_{1/2}\uparrow$ temperature. A small difference in sample temperature near $T_{1/2}\uparrow$ leads to a large difference in HS/LS mole fraction. The large error in the impact sensitivity at this temperature is positive evidence for the influence of spin crossover on the observed change in mechanical sensitivity. The decrease in the impact sensitivity of **1** from 7.50 ± 0.93 J at ambient temperature to 5.00 ± 0.66 J at 60 °C and then 3.43 ± 0.78 J at 75 °C also corresponds well to the magnetic susceptibility of compound **1** which confirms that **1**, upon heating, is fully switched to HS at 75 °C. In contrast, our measurements indicate that the impact sensitivity of **2** does not increase until heated to 75 °C. While an increase in sensitivity (due to spin transition) was expected for **1**, it is unclear why the impact sensitivity of **2** falls to 2.47 ± 0.69 J at 75 °C. There are large errors in the impact sensitivities for compound **2** at 25, 37, 48, and 60 °C, corresponding to a large range of drop heights in each data set where there were both goes and no goes (ranges of 7, 9, 13, and 14 cm for 25, 37, 48, and 60 °C, respectively, compared to a 3 cm range for 75 °C). This suggests that there may be a gradual phase change for compound **2** below 75 °C that was not detectable by DSC (the phase change due to spin transition in compound **1** was also not detected by DSC).

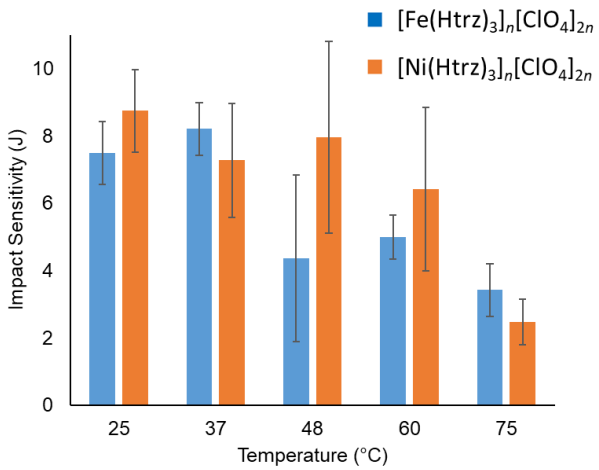

Figure 5. Impact sensitivity of $[Fe(Htrz)_3]_n[ClO_4]_{2n}$ (**1**) (blue bars) and $[Ni(Htrz)_3]_n[ClO_4]_{2n}$ (**2**) (orange bars) at different temperatures with error bars.

Table 3. Impact sensitivity data for $[Fe(Htrz)_3]_n[ClO_4]_{2n}$ (1) and $[Ni(Htrz)_3]_n[ClO_4]_{2n}$ (2) at different temperatures.

T (°C)	$[Fe(Htrz)_3]_n[ClO_4]_{2n}\cdot xH_2O$		$[Ni(Htrz)_3]_n[ClO_4]_{2n}\cdot xH_2O$	
	IS (J)[a]	x[b]	IS (J)[a]	x[b]
25[c]	7.50 ± 0.93	1.03	8.75 ± 1.23	1.26
37[c]	8.21 ± 0.78	0.90	7.28 ± 1.69	1.13
48[d]	4.36 ± 2.47	0.76	7.96 ± 2.84	0.99
60[e]	5.00 ± 0.66	0.63	6.42 ± 2.43	0.86
75[e]	3.43 ± 0.78	0.42	2.47 ± 0.69	0.65

[a]IS = impact sensitivity. [b]Equiv. of water per monomer at 25 °C was estimated from TGA experiments and the equiv. of water per monomer for the heated samples was estimated from the mass lost after 3 min on the heated anvil. [c]**1** is in the low spin state. [d]**1** is in a mixed HS/LS state at $\approx T_{1/2}\uparrow$. [e]**1** is in the high spin state.

Computational Structural and SCO Analysis. All theoretical calculations were performed using unrestricted density functional theory (uDFT) as implemented in the Gaussian 16 software package.[34] Unless otherwise noted, the uTPSSH/6-311g** level of theory was used.

Structural Analysis. The insolubility of **1** and **2** in practical solvents has precluded their X-ray single crystal molecular structure analysis. However, the extended chain structure of **3**, $[Fe(Htrz)_2(trz)]_n[BF_4]_n$, has been confirmed by X-ray powder diffraction in both the LS (300 K) and HS (420 K) states.[27] We performed energy minimization for model monomers of **1** and **2** ($[Fe(Htrz)_6]^{2+}$ and $[Ni(Htrz)_6]^{2+}$, respectively) in HS and LS states and their optimized geometries were used to determine calculated bond-lengths and interatomic distances. The optimized monomer structure models of **1** and **2** are shown in Figure 6 with the calculated bond lengths and angles listed in Tables 4 and 5 (atomic coordinates are provided in the supporting information). Polymer structures $Fe_5(Htrz)_{12}(ClO_4)_6$ (uB3LYP/6-311g**), and $Ni_5(Htrz)_{12}$ were also optimized (to predict M-M distances; M=metal) in the HS and LS states.

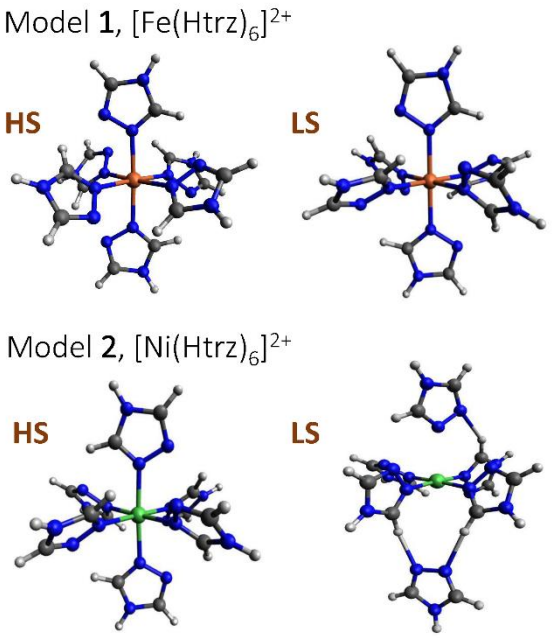

Figure 6. Optimized monomer geometries of **1** ($[Fe(Htrz)_6]^{2+}$) and **2** ($[Ni(Htrz)_6]^{2+}$) in HS and LS states (Blue = N, Grey = C, White = H, Orange = Fe, Green = Ni).

It is a common trend among SCO complexes for the HS state to have longer metal to ligand bonds than the LS state due to population of orbitals with anti-bonding character in the HS state.[35, 36] The LS structure of **1** is predicted to have an Fe-N bond length of 2.038 Å; In contrast, the predicted HS structure of **1** has lengthened Fe-N bond lengths of 2.193 Å and 2.202 Å for the equatorial and axial configuration, respectively (Table 4). These compare well with average Fe-N bond distances of 1.95(2) and 1.99(2) Å reported by Guionneau for $[Fe(NH_2trz)_3]_n(NO_3)_{2n}\cdot 2H_2O$ in the LS state[37] and to the Fe-N bond lengths of 1.991(4) and 1.998(4) Å for LS and 2.190(3) and 2.189(3) Å for HS reported in 2017 by Triki *et. al.* for $[Fe(bntrz)_3][Pt(CN)_4]\cdot H_2O$.[38] Our calculations are consistent with the literature which indicates that the Fe-N distance increases by an average of 8% upon transition from LS to HS in **1**, as expected.[1] Meanwhile, ligand bond lengths (N-N, N=C, HN-C) are relatively unaffected by the spin transition. The same trends are observed for the optimized polymeric compound, $[Fe_5(Htrz)_{12}](ClO_4)_6$, for which the distance between Fe(II) centers is 3.76 Å for LS and 3.85 Å for HS.

Table 4. Calculated average bond-lengths (Å) for models of 1 and 2. M-M distances are taken from the polymer complexes $M_5(Htrz)_{12}$.

	Model 1, $[Fe(Htrz)_6]^{2+}$		**Model 2**, $[Ni(Htrz)_6]^{2+}$	
	LS	HS	LS	HS
M-N	2.038	2.193(eq) 2.202(ax)	2.786, 4.668(eq) 1.895(ax)	2.111
N-N	1.381	1.380	1.373	1.378
N=C	1.305	1.308	1.307	1.308

HN-C	1.355	1.356	1.354	1.356
M---M $M_5(Htrz)_{12}$	3.76	3.85	N/A	4.14

Table 5. Calculated N-M-N angles (°) for models of 1 and 2 (average).

	Model 1, $[Fe(Htrz)_6]^{2+}$		**Model 2**, $[Ni(Htrz)_6]^{2+}$	
	LS	HS	LS	HS
N(eq)-M-N(ax) (90°)	89.0, 91.0 (90)	92.3, 89.9, 89.7, 88.2 (90.025)	85.9, 95.1, 98.2, 88.9 (92.025)	90.6, 87.5, 91.3, 90.6 (90)
N(ax)-M-N(ax) (90°)	89.0, 91.0 (90)	88.8, 94.4, 88.1, 88.8 (90.025)	90.1, 89.8, 89.0, 90.8 (89.925)	90.6, 87.5, 91.3, 90.6 (90)
N(ax)-M-N(ax) (180°)	180	176.3	175.9 176.0 (175.95)	177.3
N(eq)-M-N(eq) (180°)	180	176.9	N/A	177.3

A significant tetragonal distortion is required for a six coordinate d^8 metal like Ni(II) to adopt a low spin configuration.[39] An optimized geometry for the LS configuration of **2** was severely distorted, as expected. The axial metal-ligand bond distances are 1.895 Å. Only one equatorial ligand is bonded at 2.786 Å while the second is at a distance of 4.668 Å. The complex adopts a pseudo square pyramid with the Ni center 4° out of plane.

The Ni-N bond distances predicted for the HS of **2** and its polymer ($Ni_5(Htrz)_{12}$) differ on average by 4% from the Fe-N distances predicted for **1** and its polymer ($Fe_3(Htrz)_6$), and the ligand bond-distances are unaffected by the metal center, confirming that **1** and **2** are isostructural, consistent with the IR spectra (Figure 2, above and Table 6, below).

UV-Vis. UV-Vis spectra were calculated using TD-DFT with 100 states starting from the corresponding optimized HS and LS structures. The calculated spectra for models of **1** and **2** along with their corresponding experimentally measured spectra (KBr pellet; room temperature) are shown in Figure 7. The calculated absorbance of the individual contributions of **1** in HS (red) and LS (blue) states are plotted along with the experimental spectrum (black dashes) in the upper panel of Figure 7. The experimental peak at 277 nm is in good agreement with the theoretically predicted peak at 285 nm in the total spectrum. The experimental and theoretically predicted curves both reveal the shoulder and inflection point between 325 nm to 350 nm. Above 350 nm, HS contribution become dominant, thus indicating that both LS and HS states contribute to the measured spectrum at room temperature. Since the spin transition of **1** occurs near room temperature (see Figure 3, above), it is reasonable to expect a predominantly LS configuration at room temperature with a fraction of HS contribution.

The calculated spectrum of **2** is shown in the bottom panel of Figure 7. The HS state of **2** (red) features a single peak at 234 nm. The LS state of 2 (blue) features a peak at 260 nm and a shoulder at 315 nm. Meanwhile, the experimental spectrum (black dashes) exhibits a peak in absorbance at 234 nm, the same peak absorbance wavelength predicted for the HS complex.

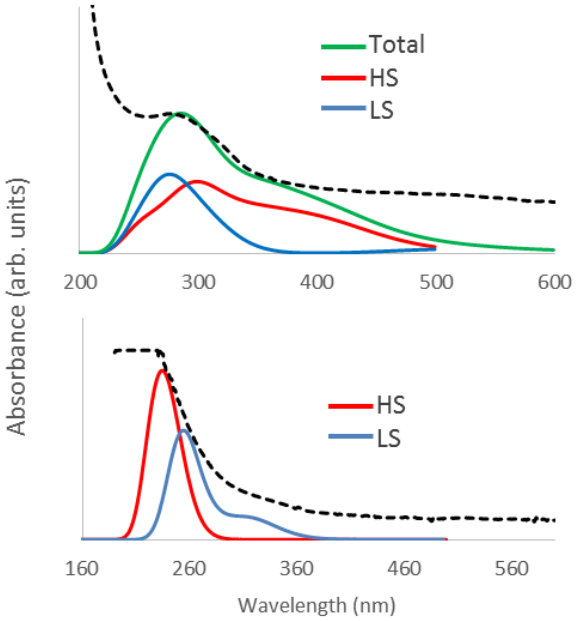

Figure 7. (**Top**) Calculated total UV-Vis spectrum (green) of complex **1** showing individual contributions from HS (red) and LS (blue) compared to experiment (dashed black). (**Bottom**) Calculated UV-Vis spectra of complex **2** for the HS state (red) and LS state (blue) compared to experiment (dashed black).

Transition Temperature. In order to verify the spin transition observed in magnetic susceptibility measurements (see Figure 3, above), the spin transition temperature of **1** was predicted by computing energies for HS and LS models optimized at temperatures varying from 250 K to 350 K. The energy as a function of temperature is plotted in Figure 8 for the LS (orange) and HS (blue) states. The HS and LS curves intersect at 305 K using a linear fit, corresponding to the theoretical transition temperature, in reasonable agreement with the $T_{1/2}$ values determined from the magnetic measurements. At temperatures below 305 K, the LS state is more stable. At temperatures above 305 K (32 °C), the HS state becomes more energetically stable.

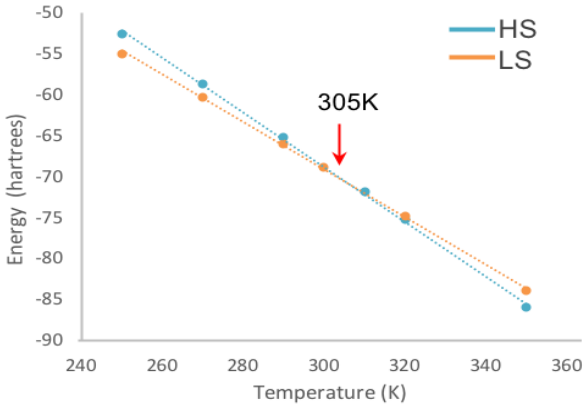

Figure 8. Calculated energies of HS (blue) and LS (orange) states of compound **1** at varying temperatures. (energy/1000 + 2717)

For compound **2**, we verified that the HS state is energetically more stable at room temperature and calculated a transition temperature to the LS state at 2269K which is well above its decomposition temperature! This is in agreement with the magnetic susceptibility data for compound **2**, where only the HS state is observed.

IR Spectra. The IR frequencies and intensities for monomer models of **1** and **2** are calculated from the respective optimized structure models (Figure 6, above) for HS and LS states. The calculated results show good agreement with the experimental spectra in Figure 2 (above); a comparison of the most relevant frequencies is presented in Table 6. All computed frequencies and intensities are provided in Table S11. The frequencies for HS and LS of compound **1** are similar. The IR spectrum in Figure 2 is similar to a previously reported IR spectrum of **1**.[30]

Table 6. Calculated IR frequencies for 1 and 2 compared to experiment.

IR frequencies (cm^{-1})	**Model 1,** $[Fe(Htrz)_6]^{2+}$		**Model 2,** $[Ni(Htrz)_6]^{2+}$	**1** Expt.	**2** Expt.
	LS	HS	HS	LS	HS
Htrz ring Combination	1536	1548		1536	
R_1 Ring stretch	1555	1527	1548	1513	1540
R_2 Ring stretch	1442	1430	1436	1420	1437
R_3 Ring stretch	1330	1318	1320	1306	1310
R_5 breathing	1146	1142	1120	1145	1121
C-H off plane	859-910	887-896	887-890	882	890
Ring torsions	618	619	618	626	626

While **1** and **2** are isostructural, they exhibit similar IR peaks and vibrational modes above 600 cm^{-1}; however, the SCO is manifested in differences below 600 cm^{-1}. Previously measured IR frequencies of pressure induced spin transitions in **1** indicate that Fe-N vibrations are shifted to lower energy in the HS state (263 cm^{-1}) compared to the LS state (299 cm^{-1}).[30] Similarly, our calculations predict a decrease in the Fe-N in-phase stretching mode from 206 cm^{-1} to 181 cm^{-1} upon transition from LS to HS. Our calculations also predict that the N-Fe-N axial bending vibration of **1** decreases from 243 cm^{-1} for LS (in agreement to the previously reported value of 220 cm^{-1})[30] and to 181 cm^{-1} for HS. The shift of the metal to ligand vibrations to lower energy in the HS state of **1** compared to the LS state is consistent with the calculated lengthening of the M-L bonds, which also correlates with the increase in sensitivity observed for the HS state.

Molecular Orbitals. The energies of frontier t_{2g} and e_g molecular orbitals (MOs) containing d-electrons reveal the differences between LS and HS states of **1**. The molecular orbital energy diagrams of **1** and **2** are displayed in Figure 9 where the d_{xy} orbital energies are set to 0. The orbitals are shown in Table S12. For the following discussion we define the energy gap as the difference in energy between either the HOMO (highest occupied molecular orbital) and LUMO (lowest unoccupied molecular orbital) for LS states or the highest doubly occupied MO and lowest singly occupied MO for HS states.

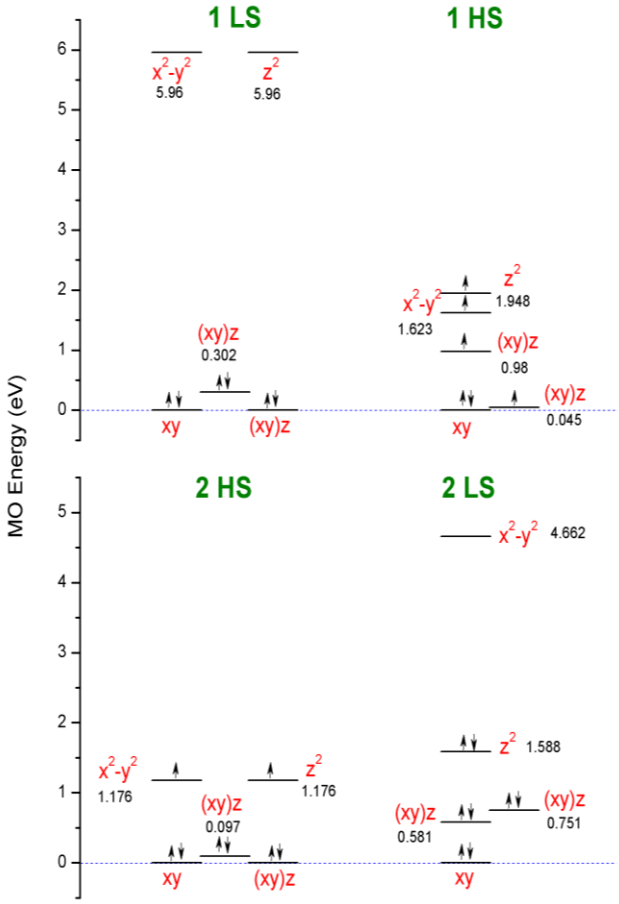

Figure 9. MO energy diagrams of d-orbitals of LS of **1** (Top left), HS of **1** (Top right), LS of **2** (Bottom left), and HS of **2** (Bottom right). For each system the d_{xy} orbital is set to 0 energy.

We start by considering the room temperature (RT) stable states, i.e. the LS state of **1** and the HS state of **2**, shown on the left side of Figure 9**.** Both RT stable electronic configurations exhibit octahedral orbital energy splitting. The octahedral splitting is in accordance with the predicted structures having equivalent metal to ligand bond distances in the equatorial (e) and axial (a) positions (see above, Table 4) and having average N-M-N angles of 90° (see above, Table 5). The LS state of **1** (top left, Figure 9), has an energy gap of 5.66 eV, which is much larger than K_BT (~0.026 eV). Promoting an electron across the gap at room temperature occurs with probability on the order of 10^{-75} according to the Boltzmann distribution, making it energetically unfavorable [to be HS] at room temperature. In contrast, the HS state of **2** (bottom left, Figure 9) has a relatively small calculated energy gap of 1.08 eV and two unpaired electrons in the two highest energy (e_g) MOs. The degeneracy of the e_g MOs in the HS state make it more stable at room temperature (compared to 2 LS) since the spin pairing energy is infinitely larger than the energy difference between e_g orbitals (spin pairing energies for first row transition metals range from 2.4 - 3.6 eV.[40] In contrast, the LS of **2** has no unpaired electrons (bottom right, Figure 9). In this case, the energy gap of 3.07 eV is larger than the spin pairing energy making the LS electronic configuration only stable at extremely high temperatures.

The right panels of Figure 9 depict the high temperature stable electronic configurations and MO energies of **1** and **2**. In both complexes, there is a change in orbital energy splitting between LS and HS states suggesting a change in geometry upon spin transition. The HS state of **1** displays MO energy splitting consistent with a compressed distortion where $d_{z(xy)}$ orbitals increase in energy with respect to the d_{xy} orbital and the d_{z2} orbital is at higher energy with respect to the d_{x2-y2} orbital. This is in agreement with the predicted structure of 1 HS having asymmetric equatorial and axial Fe-N bond lengths (see above,Table 4). Similarly, the LS of **2** indicates an MO energy splitting consistent with a square pyramid and in agreement with the predicted equatorial Ni-N bond length being larger than the axial distances (Table 4).

Conclusions and Outlook

The bond length, volume and enthalpy changes implied and calculated from spin transition in the explosive spin crossover compound $[Fe(Htrz)_3]_n[ClO_4]_{2n}$ (**1**) can potentially be harnessed to affect a useful and reversible change in sensitivity.[2] Compound **1** was synthesized and small scale sensitivity testing was performed. Its impact sensitivity was determined at various temperatures and compared to the control compound $[Ni(Htrz)_3]_n[ClO_4]_{2n}$ (**2**) that does not undergo a spin transition. As predicted, both **1** and **2** are sensitive to impact, electrostatic discharge and friction at room temperature. Our variable temperature impact sensitivity results demonstrate that the spin crossover behavior of **1** correlates closely with its impact sensitivity, with lower sensitivity in the LS state, intermediate sensitivity in the mixed LS/HS state, and higher sensitivity in the thermally accessed HS state. For comparison, the control compound **2** also exhibited an increase in sensitivity upon heating, but at a higher temperature than was required for **1**. This is the first example of using spin crossover as a mechanism to influence the initiation sensitivity of explosives in a fully reversible manner and we expect ExSCO compounds to become a new class of switchable explosive materials. We will continue to synthesize and examine the mechanical sensitivity properties of explosive spin crossover materials and explore other mechanisms to induce spin crossover, such as light, that will be suitable for practical application.

Experimental

General

Caution: Although we have not experienced any problems in handling the materials described in this paper, they are sensitive to various stimuli and should be handled with care, implementing standard safety procedures for handling energetic and explosive materials.

Unless otherwise noted, all starting materials were obtained from commercial sources and used as received. Elemental analyses of energetic materials were performed using a PerkinElmer series II 2400 CHNS/O analyzer. Elemental analyses of compound **3** was performed by Atlantic Microlab, Inc. in Norcross, GA. IR spectra were recorded using a Thermo Scientific Nicolet iS5 FTIR spectrophotometer. UV-Vis experiments were performed using a Hewlett Packard 8453 (G1103A) Diode-Array UV/Vis spectrophotometer on solid state samples in KBr pellets. Thermogravimetric Analysis (TGA) was performed using a TA Instruments TGA Q5000IR.

Mechanical Sensitivity. Impact sensitivity was measured by using a drop hammer LANL Explosives Research Laboratory (ERL) type 12b test (no grit) using a 0.8 kg striker, 2.5 kg weight and the Neyer D-Optimal method to determine the 50% drop height using a go/no-go threshold level of 105 dB (see supplementary information for more details). The temperature of the anvil was controlled by a LANL designed aluminum collar, fitted onto the anvil with two Viton O-rings that contained a channel for ethylene glycol from a temperature controlled chiller to flow through (Figure 4). The temperature of the strikers was controlled using an oven. The samples were set on the anvil for 2-3 min before impact to equilibrate to the temperature of the anvil, then the heated strikers were placed directly on the samples prior to impact by the drop hammer. Friction sensitivity were performed with a BAM friction instrument determining the 50% load using the Neyer D-Optimal method. Electrostatic discharge/spark sensitivity testing was performed on an ABL ESD instrument to determine threshold initiation level (TIL). Thermal decomposition temperatures were measured by DSC (TA Instruments Q2000 DSC) in hermetically sealed aluminum pans that contain a pinhole lid. A typical analysis utilizes approximately 1 mg of sample with 50 mL/min ultrahigh purity nitrogen purge gas at a thermal ramp rate of 10 °C/min. All cyclic DSC data was recorded at a thermal ramp rate of 2.5 °C/min. All sensitivity data is referenced to a PETN standard.

Monitoring Water Content. Monitoring of water content for compounds **1** and **2** was accomplished in two different

ways: (1) by comparing the weight of samples before and after heating on the impact sensitivity anvil to determine water loss and (2) by using TGA experiments to determine total H_2O content.

Magnetic Measurements. The samples of **1** and **2**, diluted with KBr, were precisely weighed and packed in the plastic drinking straws with 10 mg quartz wool. The DC moment magnetic measurements were performed on the Quantum Design MPMS XL magnetometer. Diamagnetic corrections using Pascal constants were introduced. $[Fe(Htrz)_2(trz)]_n[BF_4]_n$ (**3**) was synthesized according to a literature procedure[26] for verification of our magnetism measurement sample preparation methods.

$[Fe(Htrz)_3]_n[ClO_4]_{2n}$ (1). **1** was prepared according to a previously reported procedure:[14] To a flask charged with $Fe(ClO_4)_2{\cdot}6H_2O$ (1.451 g, 4.000 mmol) and ascorbic acid (23.9 mg, 0.136 mmol) was added MeOH (200 mL) with stirring. This resulted in the dissolution of the metal salt to form a yellow solution, quickly followed by the dissolution of the ascorbic acid, which caused a change to a clear and colorless solution. A solution of 1,2,4-triazole (833.7 mg, 12.07 mmol) in MeOH (200 mL) was added and the reaction mixture was stirred for 30 min. The solution remained clear and colorless. The solvent was then removed in a rotary evaporator while rotating in a water bath set to 60 °C. Off white powder precipitated from the solution upon concentration, which turned purple upon cooling to room temperature. The purple powder was further dried *in vacuo* for 3.5 h while heated to 65 °C (1.80 g, 98% yield). The weight of the sample was monitored for absorption of H_2O due to exposure to air prior to analysis. Anal. Calc'd for $C_6H_{11.06}Cl_2FeN_9O_{9.03}$ (**1**·1.03H_2O): C, 15.00; H, 2.32; N, 26.24. Found: C, 15.39; H, 2.34; N, 26.02. UV-Vis (KBr, a.u.): 288 (br). IR (KBr pellet, cm^{-1}): 626 (s), 882 (w), 954 (w), 999 (w), 1107 (s), 1145 (s), 1306 (w), 1420 (w), 1513 (w), 1536 (w), 2814 (w), 2894 (w), 3006 (m), 3142 (s), 3377 (w).

$[Ni(Htrz)_3]_n[ClO_4]_{2n}$ (2). **2** was prepared similarly to compound **1**: To a flask charged with $Ni(ClO_4)_2{\cdot}6H_2O$ (1.464 g, 4.004 mmol) was added MeOH (200 mL) with stirring to dissolve all the solid. A solution of 1,2,4-triazole (833.0 mg, 12.06 mmol) in MeOH (200 mL) was then added. This resulted in a color change of the green solution to blue. The reaction mixture was stirred for 30 min, upon which there was no further change. The solvent was then removed in a rotary evaporator while rotating in a water bath set to 60 °C. The resulting purple powder was further dried *in vacuo* for 3.5 h while heated to 65 °C (1.79 g, 96% yield). The weight of the sample was monitored for absorption of H_2O due to exposure to air prior to analysis. Anal. Calc'd for $C_6H_{11.52}Cl_2N_9NiO_{9.26}$ (**2**·1.26H_2O): C, 14.78; H, 2.38; N, 25.86. Found: C, 14.72; H, 2.43; N, 25.79. UV-Vis (KBr, a.u.): 297 (sh). IR (KBr pellet, cm^{-1}): 626 (s), 890 (w), 959 (w), 1108 (s), 1121 (s), 1310 (m), 1437 (w), 1540 (w), 2828 (w), 2903 (w), 3005 (m), 3143 (m), 3403 (m).

$[Fe(Htrz)_2(trz)]_n[BF_4]_n$ (3). **3** was prepared according to a previously reported procedure:[26] To a clear and colorless solution of $Fe(BF_4)_2{\cdot}6H_2O$ (843 mg, 2.50 mmol) in H_2O (5 mL) was added a slurry of 1,2,4-triazole (520 mg, 7.54 mmol) in EtOH (3 mL). The reaction immediately formed a suspension of fine purple powder. After stirring for 14 h, the reaction was allowed to stand for another 10 h. There was no visible change of the fine purple suspension during this time. The purple solid was collected on a 1.2 μm nylon membrane filter, washed with EtOH and dried *in vacuo* 2 h while heated to 65 °C (471 mg, 34% yield). **3** does not absorb H_2O once dry. Anal. Calc'd for $C_6H_8BF_4FeN_9$: C, 20.66; H, 2.31; N, 36.14. Found: C, 19.85; H, 2.35; N, 33.88. Note: our CHN analysis is consistent with a formulation in which a small amount of $[Fe(Htrz)_3]_n[BF_4]_n$, a compound which is typically generated when the same reaction is done in MeOH, is formed.[26] For example, the Anal. Calc'd for $C_{36}H_{49}B_7F_{28}Fe6N_{54}$ ($\{[Fe(Htrz)_2(trz)][BF_4]\}_{5n}\{[Fe(Htrz)_3][BF_4]\}_n$) is C, 19.83; H, 2.26; N, 34.68, a good match for our results. IR (KBr pellet, cm^{-1}): 524 (m), 633 (m), 680 (m), 829(w), 867 (m), 910 (w), 978 (m), 1070 (s), 1145 (s), 1163 (s), 1189 (m), 1221 (w), 1285 (m), 1308 (m), 1453 (m), 1496 (m), 1534 (m), 2457 (w), 2535 (m), 2623 (m), 2668 (m), 2698 (m), 2748 (m), 2864 (m), 2919 (m), 3013 (s), 3102 (s), 3179 (s).

ASSOCIATED CONTENT

The supporting information is available free of charge via the Internet at http://pubs.acs.org and includes the following information:

IR spectra of **1**-**3**
Magnetism data for **2**
Thermal analysis data for **1**-**3**
Explosive sensitivity data for **1** and **2**
Theory data for models of **1** and **2**

AUTHOR INFORMATION

Corresponding Authors

* tdnguyen@lanl.gov
* veauthier@lanl.gov

Present Addresses

§Lawrence Livermore National Laboratory

Author Contributions

The manuscript was written through contributions of all authors. All authors have given approval to the final version of the manuscript.

ACKNOWLEDGMENT

We thank Brent Faulkner, Bob Houlton, and Lisa Kay for their work on the VT impact collar design and the High Explosives Science & Technology group's analytical team for data collection. Research presented in this article was supported by the Laboratory Directed Research and Development program of Los Alamos National Laboratory under project number ER20180369. Los Alamos National Laboratory is operated by Triad National Security, LLC, for the National Nuclear Security Administration of U.S. Department of Energy (Contract No. 89233218CNA000001). T.-A. D. Nguyen is supported by an Agnew National Security Postdoctoral Fellowship. This research used resources provided by the LANL Institutional Computing (IC) Program.

REFERENCES

1. Guionneau, P., Crystallography and spin-crossover. A view of breathing materials. *Dalton Trans.* **2014**, *43* (2), 382-393.

2. Gutlich, P.; Garcia, Y.; Goodwin, H. A., Spin crossover phenomena in Fe(II) complexes. *Chem. Soc. Rev.* **2000,** *29* (6), 419-427.

3. Olivier, R., Triazole-Based One-Dimensional Spin-Crossover Coordination Polymers. *Chem. Eur. J.* **2012,** *18* (48), 15230-15244.

4. Aromí, G.; Barrios, L. A.; Roubeau, O.; Gamez, P., Triazoles and tetrazoles: Prime ligands to generate remarkable coordination materials. *Coord. Chem. Rev.* **2011,** *255* (5), 485-546.

5. Kahn, O., Spin-crossover molecular materials. *Curr. Opin. Solid St. M.* **1996,** *1* (4), 547-554.

6. Renz, F., Physical and chemical induced spin crossover. *J. Phys. Conf. Ser.* **2010,** *217*, 012022.

7. Qi, Y.; Müller, E. W.; Spiering, H.; Gütlich, P., The effect of a magnetic field on the high-spin α low-spin transition in $[Fe(phen)_2(NCS)_2]$. *Chem. Phys. Lett.* **1983,** *101* (4), 503-505.

8. Kimura, S.; Narumi, Y.; Kindo, K.; Nakano, M.; Matsubayashi, G.-e., Field-induced spin-crossover transition of $[Mn^{III}(taa)]$ studied under pulsed magnetic fields. *Phys. Rev. B* **2005,** *72* (6), 064448.

9. Gütlich, P.; Ksenofontov, V.; Gaspar, A. B., Pressure effect studies on spin crossover systems. *Coord. Chem. Rev.* **2005,** *249* (17), 1811-1829.

10. Gütlich, P.; Hauser, A., Thermal and light-induced spin crossover in iron(II) complexes. *Coord. Chem. Rev.* **1990,** *97*, 1-22.

11. Halcrow, M. A., Structure:function relationships in molecular spin-crossover complexes. *Chem. Soc. Rev.* **2011,** *40* (7), 4119-4142.

12. Pittala, N.; Thétiot, F.; Charles, C.; Triki, S.; Boukheddaden, K.; Chastanet, G.; Marchivie, M., An unprecedented trinuclear Fe^{II} triazole-based complex exhibiting a concerted and complete sharp spin transition above room temperature. *Chem. Com.* **2017,** *53* (59), 8356-8359.

13. Sugahara, A.; Kamebuchi, H.; Okazawa, A.; Enomoto, M.; Kojima, N., Control of Spin-Crossover Phenomena in One-Dimensional Triazole-Coordinated Iron(II) Complexes by Means of Functional Counter Ions. *Inorganics* **2017,** *5* (3), 50.

14. Krober, J.; Codjovi, E.; Kahn, O.; Groliere, F.; Jay, C., A spin transition system with a thermal hysteresis at room temperature. *J. Am. Chem. Soc.* **1993,** *115* (21), 9810-9811.

15. Bausk, N. V.; Érenburg, S. B.; Mazalov, L. N.; Lavrenova, L. G.; Ikorskii, V. N., Electronic and spatial structure of spin transition iron(II) tris(4-amino-1,2,4-triazole) nitrate and perchlorate complexes. *J. Struct. Chem.* **1994,** *35* (4), 509-516.

16. Garcia, Y.; van Koningsbruggen, P. J.; Lapouyade, R.; Rabardel, L.; Kahn, O.; Wieczorek, M.; Bronisz, R.; Ciunik, Z.; Rudolf, M. F., Synthesis and spin-crossover characteristics of polynuclear 4-(2′-hydroxy-ethyl)-1,2,4-triazole Fe(II) molecular materials. *C. R. Acad. Sci. Ser. IIC Chem.* **1998,** *1* (8), 523-532.

17. Roubeau, O.; Castro, M.; Burriel, R.; Haasnoot, J. G.; Reedijk, J., Calorimetric Investigation of Triazole-Bridged Fe(II) Spin-Crossover One-Dimensional Materials: Measuring the Cooperativity. *J. Phys. Chem. B* **2011,** *115* (12), 3003-3012.

18. Roubeau, O.; Alcazar Gomez, J. M.; Balskus, E.; Kolnaar, J. J. A.; Haasnoot, J. G.; Reedijk, J., Spin-transition behaviour in chains of Fe^{II} bridged by 4-substituted 1,2,4-triazoles carrying alkyl tails. *New J. Chem.* **2001,** *25* (1), 144-150.

19. Robinson, W. R., Perchlorate salts of metal ion complexes: Potential explosives. *J. Chem. Educ.* **1985,** *62* (11), 1001.

20. Espenson, J. H., The Problem and Perversity of Perchlorate. In *Perchlorate in the Environment*, Urbansky, E. T., Ed. Springer US: Boston, MA, 2000; pp 1-7.

21. Cady, H. H.; Smith, L. C., *Studies on the polymorphs of HMX*. Los Alamos Scientific Laboratory of the University of California, Los Alamos, New Mexico: Los Alamos, N.M., 1962; p 50.

22. Asay, B. W.; Henson, B. F.; Smilowitz, L. B.; Dickson, P. M., On the Difference in Impact Sensitivity of Beta and Delta HMX. *J. Energetic Mater.* **2003,** *21* (4), 223-235.

23. Gütlich, P.; Gaspar, A. B.; Garcia, Y., Spin state switching in iron coordination compounds. *Beilstein J. Org. Chem* **2013,** *9*, 342-391.

24. Boča, R.; Boča, M.; Dlháň, L.; Falk, K.; Fuess, H.; Haase, W.; Jaroščiak, R.; Papánková, B.; Renz, F.; Vrbová, M.; Werner, R., Strong Cooperativeness in the Mononuclear Iron(II) Derivative Exhibiting an Abrupt Spin Transition above 400 K. *Inorg. Chem.* **2001,** *40* (13), 3025-3033.

25. Sone, K.; Fukuda, Y., Thermochromism of Nickel(II) Chelates in Solution. In *Inorganic Thermochromism*, Jorgensen, C. K.; Lappert, M. F.; Lippard, S. J.; Margrave, J. L.; Niedenzu, K.; Nöth, H.; Parry, R. W.; Yamatera, H., Eds. Springer Berlin Heidelberg: Berlin, Heidelberg, 1987; pp 43-71.

26. Krober, J.; Audiere, J.-P.; Claude, R.; Codjovi, E.; Kahn, O.; Haasnoot, J. G.; Groliere, F.; Jay, C.; Bousseksou, A., Spin Transitions and Thermal Hysteresis in the Molecular-Based Materials $[Fe(Htrz)_2(trz)](BF_4)$ and $[Fe(Htrz)_3](BF_4)2{\cdot}H_2O$ (Htrz = 1,2,4-4*H*-triazole; trz = 1,2,4-triazolato). *Chem. Mater.* **1994,** *6* (8), 1404-1412.

27. Arnaud, G.; Philippe, N.; Pierre, B.; Céline, E.; Denise, M.; Stanislav, P.; Eric, L.; Jean-François, L.; Philippe, G., Crystal Structures and Spin Crossover in the Polymeric Material $[Fe(Htrz)_2(trz)](BF_4)$ Including Coherent-Domain Size Reduction Effects. *Eur. J. Inorg. Chem.* **2013,** *2013* (5-6), 796-802.

28. Haasnoot, J. G.; Groeneveld, W. L., Complexes of Transition Metal(II) Thiocyanates with 1,2,4-Triazole. *Z. Naturforsch.* **1977,** *32b* (5), 533-536.

29. Haasnoot Jaap, G.; Vos, G.; Groeneveld Willem, L., 1,2,4-Triazole Complexes, III Complexes of Transition Metal(II) Nitrates and Fluoroborates. *Z. Naturforsch.* **1977,** *32b* (12), 1421-1430.

30. Smit, E.; Waal, D.; Heyns, A., Spin-transition complexes $[Fe(Htrz)_3](ClO_4)_2$ and $[Fe(NH_2trz)_3](ClO_4)_2$. I. FT-IR spectra of a low pressure and a low temperature phase transition. *Materials Research Bulletin* **2000,** *35*, 1697-1707.

31. Shakirova, O. G.; Shvedenkov, Y. G.; Naumov, D. Y.; Beizel', N. F.; Sheludyakova, L. A.; Dovlitova, L. S.; Malakhov, V. V.; Lavrenova, L. G., $^1A_1 \Leftrightarrow {}^5T_2$ Spin Transition in Heterometallic Solid Phases $Fe_xNi_{1-x}(Htrz)_3(NO_3)_2 \cdot H_2O$ (Htrz = 1,2,4-Triazole). *J. Struct.* **2002,** *43* (4), 601-607.

32. Oxygen balance: Ω_{CO_2} = (−1600/molecular mass)*(2(# of C atoms) + (# of H atoms)/2 + x(# of M atoms) − (#of O atoms)); Ω_{CO} = (−1600/molecular mass)*((# of C atoms) + (# of H atoms)/2 + x(# of M atoms) − (#of O atoms)), where x=1 for Ni and x = 1.5 for Fe, assuming that NiO and Fe_2O_3 are the most stable and abundant oxides for Ni and Fe, respectively.

33. Impact sensitivity: $IS = m{\cdot}g{\cdot}H_{50}$, where m = 2.5 kg and g = 9.8 $m{\cdot}s^{-2}$.

34. Frisch, M. J.; Trucks, G. W.; Schlegel, H. B.; Scuseria, G. E.; Robb, M. A.; Cheeseman, J. R.; Scalmani, G.; Barone, V.; Petersson, G. A.; Nakatsuji, H.; Li, X.; Caricato, M.; Marenich, A. V.; Bloino, J.; Janesko, B. G.; Gomperts, R.; Mennucci, B.; Hratchian, H. P.; Ortiz, J. V.; Izmaylov, A. F.; Sonnenberg, J. L.; Williams; Ding, F.; Lipparini, F.; Egidi, F.; Goings, J.; Peng, B.; Petrone, A.; Henderson, T.; Ranasinghe, D.; Zakrzewski, V. G.; Gao, J.; Rega, N.; Zheng, G.; Liang, W.; Hada, M.; Ehara, M.; Toyota, K.; Fukuda, R.; Hasegawa, J.; Ishida, M.; Nakajima, T.; Honda, Y.; Kitao, O.; Nakai, H.; Vreven, T.; Throssell, K.; Montgomery Jr., J. A.; Peralta, J. E.; Ogliaro, F.; Bearpark, M. J.; Heyd, J. J.; Brothers, E. N.; Kudin, K. N.; Staroverov, V. N.; Keith, T. A.; Kobayashi, R.; Normand, J.; Raghavachari, K.; Rendell, A. P.; Burant, J. C.; Iyengar, S. S.; Tomasi, J.; Cossi, M.; Millam, J. M.; Klene, M.; Adamo, C.; Cammi, R.; Ochterski, J. W.; Martin, R. L.; Morokuma, K.; Farkas, O.; Foresman, J. B.; Fox, D. J. *Gaussian 16 Rev. C.01*, Wallingford, CT, 2016.

35. Reger, D. L.; Little, C. A.; Smith, M. D.; Long, G. J., Solid-State Structural and Magnetic Investigations of {M[HC(3,5-$Me_2pz)_3]_2$}$(BF_4)_2$ (M = Fe, Co, Ni, Cu): Observation of a Thermally Induced Solid-State Phase Change Controlling an Iron(II) Spin-State Crossover. *Inorg. Chem.* **2002,** *41* (17), 4453-4460.

36. Reger, D. L.; Little, C. A.; Rheingold, A. L.; Lam, M.; Liable-Sands, L. M.; Rhagitan, B.; Concolino, T.; Mohan, A.; Long, G. J.; Briois, V.; Grandjean, F., A Synthetic, Structural, Magnetic, and Spectral Study of Several {Fe[tris(pyrazolyl)methane$]_2$}$(BF_4)_2$ Complexes: Observation of an Unusual Spin-State Crossover. *Inorg. Chem.* **2001,** *40* (7), 1508-1520.

37. Grosjean, A.; Daro, N.; Kauffmann, B.; Kaiba, A.; Letard, J.-F.; Guionneau, P., The 1-D polymeric structure of the $[Fe(NH_2trz)_3](NO_3)_2{\cdot}nH_2O$ (with n = 2) spin crossover compound proven by single crystal investigations. *Chem. Com.* **2011,** *47* (45), 12382-12384.

38. Pittala, N.; Thétiot, F.; Triki, S.; Boukheddaden, K.; Chastanet, G.; Marchivie, M., Cooperative 1D Triazole-Based Spin Crossover Fe^{II} Material With Exceptional Mechanical Resilience. *Chem. Mater.* **2017,** *29* (2), 490-494.

39. Thies, S.; Bornholdt, C.; Köhler, F.; Sönnichsen, F.; Näther, C.; Tuczek, F.; Herges, R., Coordination-Induced Spin Crossover (CISCO) through Axial Bonding of Substituted Pyridines to Nickel-Porphyrins: σ-Donor versus π-Acceptor Effects. *Chemistry* **2010,** *16*, 10074-83.

40. Vanquickenborne, L. G.; Haspeslagh, L., On the meaning of spin-pairing energy in transition-metal ions. *Inorg. Chem.* **1982,** *21* (6), 2448-2454.

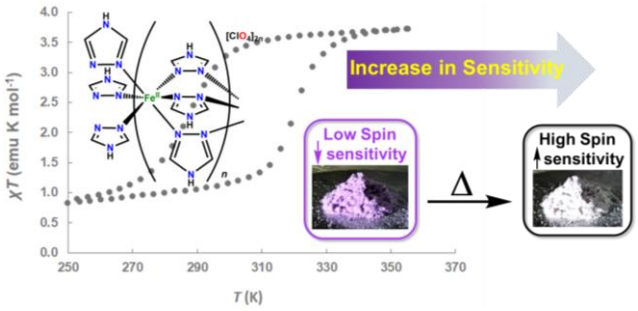

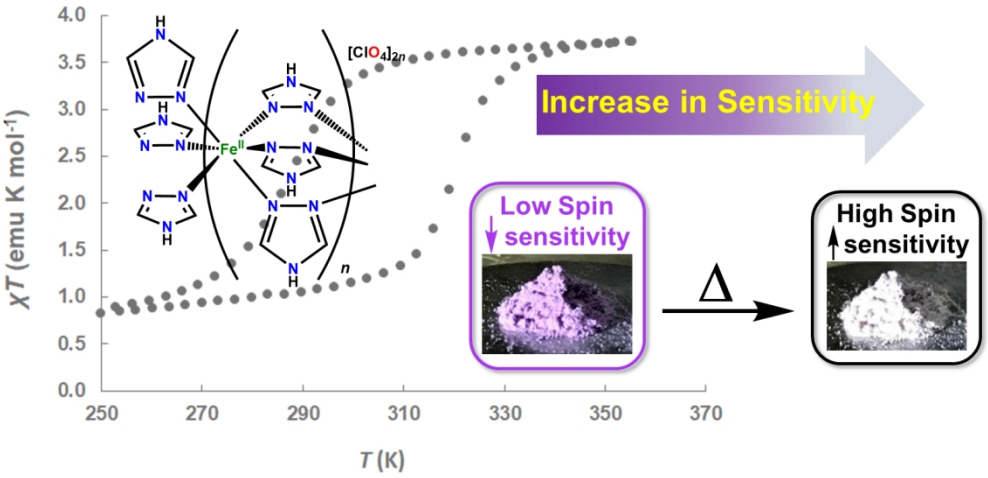
Increase in Sensitivity
Low Spin
sensitivity
High Spin
sensitivity
Δ
χT (emu K mol-1)
T (K)
[ClO4]2n
Fe II
n